Cooperative Base Line Interferometer for SWaP Optimized Direction Finding Receivers

SOUNAK SAMANTA, Member, IEEE
Defence Electronics Research Laboratory (DLRL-DRDO), Hyderabad, Telangana, India

MRITYUNJOY CHAKRABORTY, Senior Member, IEEE
Indian Institute of Technology Kharagpur, Kharagpur, West Bengal, India

Base line interferometer (BLI) is a popular direction of arrival (DOA) estimation technique for electronic warfare applications. For size, weight, and power (SWaP) optimized realization of the BLI, switched mode of operation is preferred which uses fewer number of receiver channels than the number of antenna elements and switches them among the antenna-pairs in a phased manner. Such switched operation, however, results in a suboptimal performance, since, as shown in this article, it reduces the tolerable phase-error margin (TPM), and thus, produces more erroneous DOA estimates. To overcome this, we propose a three-antenna BLI algorithm named as *Cooperative BLI (Co-BLI) triplet* which provides more TPM while maintaining high DOA estimation accuracy. This improvement comes at the cost of slight increase in implementation resources. To increase the estimation accuracy further, we next extend the proposed Co-BLI to the case of more number of antennas. For this, we also propose a way to reduce the number of antennas to form a higher order array and derive the expressions for all inter-element distances. For real-time operation, we develop a *Mapping-based Cooperative Ambiguity Table* (M-CAT): a look-up-table based implementation scheme where we show that by storing just a few combinations of the input ranges, one can estimate any DOA within the given field-of-view accurately, thus facilitating high throughput hardware implementation avoiding complex computations. The proposed algorithm has been validated through extensive MATLAB simulation studies and implemented in FPGA based real-time hardware.

Manuscript received 13 April 2023; revised 9 August 2023; accepted 2 October 2023. Date of publication 13 October 2023; date of current version 9 February 2024.

DOI. No. 10.1109/TAES.2023.3323920

Refereeing of this contribution was handled by H. Mir.

Authors' addresses: Sounak Samanta is with the Defence Electronics Research Laboratory (DLRL-DRDO), Hyderabad 500005, India, E-mail: (sounak2@yahoo.co.in); Mrityunjoy Chakraborty is with the Indian Institute of Technology Kharagpur, Kharagpur 721302, India, E-mail: (mrityun@ece.iitkgp.ac.in). *(Corresponding author: Mrityunjoy Chakraborty.)*

I. INTRODUCTION

Direction of arrival (DOA) estimation for locating unknown hostile radar installations is one of the major tasks in electronic support (ES) applications [1], [2]. In general, DOA estimation techniques use amplitude, phase, frequency, or time of arrival of the intercepted radar signal to estimate the DOA. Out of these, phase-based DOA estimators are popular due to their inherent immunity to noise. Literature is replete with several such techniques like base line interferometer (BLI), correlative interferometer (CI), multiple signal classification (MUSIC), estimation of signal parameters via rotational invariance technique (ESPRIT) and their variants, etc [3], [4]. Of these, the BLI plays a crucial role in ES applications due to its computational simplicity, especially as modern ES receivers have to operate under very limited response time (typically of the order of few hundreds of nanoseconds). Research has been going on for years to increase the accuracy of DOA estimates in a BLI array while keeping probability of ambiguity to a minimum. Goodwin [5] provided optimum array-configurations for three and four-antenna interferometers minimizing the probability of ambiguity. He resolved phase ambiguity of the longer four-antenna array using shorter three-antenna subarrays through an ambiguity diagram. Sundaram et al. [6] proposed a modulo conversion method in a coprime array. They considered consecutive inter-element baselines and resolved phase ambiguity in the longest of them using shorter inter-element spacings. However, this results in suboptimal BLI array design as end-to-end element spacing is not considered for DOA estimation. Lee et al. [7] modified Jacob's phase space method using axis-transform technique and found an array spacing that withstands maximum phase error occurring in an interferometer direction finding (DF) system. However, for the proposed phase sample-space diagram, a graphical method is difficult to visualize and extend beyond more than four antennas. In a separate work, Lee et al. [8] devised a phase-difference diagram as a substitute to it. Recently, Horng [9] proposed a four-element array-based phase interferometer system and the phase ambiguity is resolved between end-to-end elements using shorter three-element subarrays based on Goodwin's subarray cascade [5], for which a computationally efficient sorted essential ambiguity table was proposed in place of the ambiguity diagrams of [5].

Another challenge in the context of ES is reduction of size, weight, and power (SWaP). This SWaP requirement is obvious for the airborne platform, where additional size and weight come as penalty in fuel consumption. The ground and naval-based systems also demand the same so that height of the receiver can be increased resulting in enhanced line-of-sight (LOS) distance with the radar transmitter and thereby, providing greater reconnaissance coverage. The DF algorithms, as mentioned in [5], [6], [7], [8], and [9], use the same number of receiver-channels as that of the antennas and hence, do not cover any SWaP-aware aspect. Few researchers [10], [11] have reported switched-element

DF, where SWaP is optimized by reducing the number of receiver channels keeping number of antennas same. However, they have considered beamformer based and not BLI-based DF algorithms, where the former is known to require considerable amount of processing time. In [12], the usage of a switch in a four-element interferometer array with four channels reduces one hardware channel resulting into three channels. However, the proposed scheme cannot be generalized to reduce to dual channel or handle more than three channels. Moreover, it shows improvements in DF accuracy using correlation method, a search-based DOA estimation scheme that has more response time than BLI.

In this article, we consider the BLI algorithm from the standpoint of SWaP optimized ES receivers equipped with reduced number of receiver-channels (say, dual-channel) in switched-element (SE) configuration. For this, we start with a linear, switched array of three antennas and first show that the existing BLI techniques [3], [4], [5], [6], [7], [8], [9], [12] provide suboptimal performance in this case. This is because while, for attaining highest DF estimation accuracy, it is required to take the estimate from the longest baseline, our analysis shows that the tolerable phase error margin (TPM) in the longest baseline reduces as we move from the nonswitched case to the switched case. To counter this, we next propose a collaborative approach where a certain parameter solved from the phase ambiguity equations of the shorter baselines is reused in the equations involving the longest baseline. We show that in a such case, the TPM in the longest baseline does not drop but remains at the same level as in the nonswitched case, and thus, the probability of ambiguity also remains at the minimum. We term the array as the *cooperative BLI (Co-BLI) triplet*. We next generalize this approach to the case of more number of antennas to achieve higher DOA estimation accuracy while maintaining the same field-of-view and TPM. For this, we also propose a way to reduce the number of antennas while forming a higher order array and derive the expressions for all inter-element distances. For real-time operation, we develop a *mapping-based cooperative ambiguity table (M-CAT)*: a look-up-table based implementation scheme where we show that by storing a few combinations of the input ranges, one can estimate any DOA within the given field-of-view accurately, thus facilitating high throughput hardware implementation avoiding complex computations. The claimed advantages of the proposed scheme are validated by extensive MATLAB-based simulation studies. The Co-BLI logic is also coded in very high speed integrated circuit hardware decriptive language (VHDL) and implemented in field-programmable-gate-array (FPGA) based realtime hardware. The prototype hardware is tested and validated in a radiation-mode environment inside a laboratory.

II. BACKGROUND

BLI arrays use pairs of directional antennas to form baselines. To start with, we consider an array having only two antennas. The true phase difference, say, $\Delta\psi_{ij}^T$ across a baseline distance d_{ij} between the antennas (say, i and j) for a certain DOA θ at a wavelength λ is expressed as

$$\Delta\psi_{ij}^T = \frac{2\pi}{\lambda}\, d_{ij}\, \sin\theta. \tag{1}$$

Taking into account *DOA estimate error* $\Delta\theta$ caused by phase error $e_{\Delta\psi_{ij}}$ in measuring $\Delta\psi_{ij}^T$, we get $\Delta\psi_{ij}^T + e_{\Delta\psi_{ij}} = \frac{2\pi}{\lambda}\, d_{ij}\, \sin(\theta + \Delta\theta)$. For a small $\Delta\theta$, this leads to

$$\Delta\theta \approx \frac{e_{\Delta\psi_{ij}}\,\lambda}{2\pi\, d_{ij}\cos\theta}. \tag{2}$$

The baseline distance d_{ij} is selected such that $\Delta\psi_{ij}^T$ confines its value from 0 to 2π for a certain predefined range of θ (say, from θ_1 to θ_2), termed as *total field-of-view* (FOV_T). Clearly, at a given wavelength λ, a smaller value of d_{ij} yields wider FOV_T. A low value of d_{ij} for a given wide FOV_T, termed as *virtual baseline* d_{vsb} here, is not, however, practically feasible due to two factors. First, wide-band antennas usually have larger apertures, thus requiring certain minimum distance of separation between them. Second, since the baseline distance d_{ij} and DF error $\Delta\theta$ are inversely related, as in (2), DF accuracy is poor when d_{ij} is small. Therefore, it is necessary to increase the baseline distance d_{ij} in order to accommodate practical wide-band antennas and obtain the required high DF accuracy while maintaining the same FOV_T. Increasing d_{ij}, however, results in $\Delta\psi_{ij}^T$ exceeding its range $[0, 2\pi]$, thereby leading to ambiguity in phase measurement as the measured phase difference, say, $\Delta\psi_{ij}$ is always limited to $[0, 2\pi]$. The relationship between $\Delta\psi_{ij}$ and $\Delta\psi_{ij}^T$ is easily seen to be given by

$$\Delta\psi_{ij} = \Delta\psi_{ij}^T + e_{\Delta\psi_{ij}} - 2\pi K_{ij} \tag{3}$$

where $e_{\Delta\psi_{ij}}$ is the measurement error associated with the differential phase and K_{ij} is a positive integer (to be determined) that restricts $\Delta\psi_{ij}$ to the range $[0, 2\pi]$. For determination of K_{ij}, two antennas are, however, not enough and one needs more than two antennas forming a BLI array. A three-element BLI array is shown in Fig. 1. Here, we consider any two of the three possible baselines, with baseline distances $d_\alpha = \alpha d_{\text{vsb}}$ and $d_\beta = \beta d_{\text{vsb}}$ for some integers α, β that are coprime and $0 < \alpha < \beta$. To simplify the notation, we replace "ij" in the suffix of all the variables appearing in (3) by either α or β, to obtain the following equations for $\alpha : \beta$ ratio-ed BLI:

$$\Delta\psi_\alpha = \Delta\psi_\alpha^T + e_{\Delta\psi_\alpha} - 2\pi K_\alpha, \tag{4a}$$

$$\Delta\psi_\beta = \Delta\psi_\beta^T + e_{\Delta\psi_\beta} - 2\pi K_\beta, \tag{4b}$$

where K_α and K_β assume values from 0 to $\alpha - 1$ and 0 to $\beta - 1$, respectively, as from (1) and from the definition of d_{vsb}, the ranges of $\Delta\psi_\alpha^T$ and $\Delta\psi_\beta^T$ are now $[0, 2\pi\alpha]$ and $[0, 2\pi\beta]$, respectively. In the following, we introduce certain BLI-related terminologies along the lines of [3], [4], [5], and [9] which are useful in the subsequent treatment.

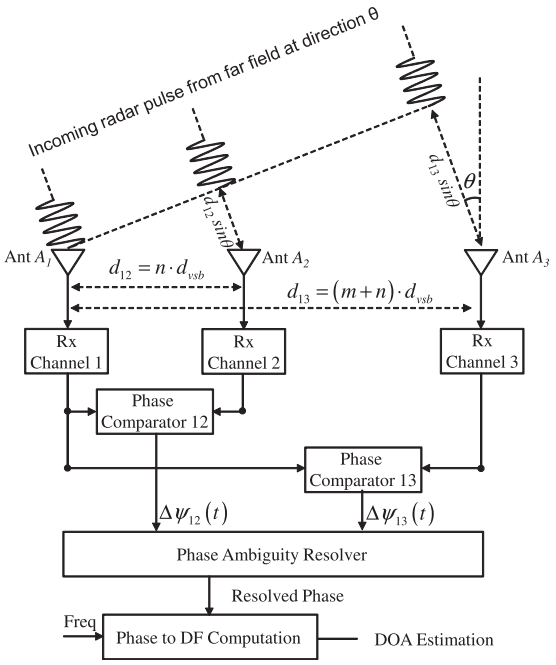

Fig. 1. Block diagram of fixed or nonswitched three-element BLI array.

A. Array Phase Integer $I_{\alpha,\beta}$ and Ambiguity Resolving Number $R_{\alpha,\beta}$

The *array phase integer (API)* [9] is defined as

$$I_{\alpha,\beta} = \alpha K_\beta - \beta K_\alpha. \tag{5}$$

We also define a related term, *ambiguity resolving number (ARN)*, as

$$R_{\alpha,\beta} = \frac{\beta\Delta\psi_\alpha - \alpha\Delta\psi_\beta}{2\pi}. \tag{6}$$

Clearly, from (1), (4), (5), and (6),

$$R_{\alpha,\beta} = I_{\alpha,\beta} + \Delta R_{\alpha,\beta} \tag{7}$$

where $\Delta R_{\alpha,\beta} = \frac{\beta e_{\Delta\psi_\alpha} - \alpha e_{\Delta\psi_\beta}}{2\pi}$. The term $\beta e_{\Delta\psi_\alpha} - \alpha e_{\Delta\psi_\beta}$ is termed as *total effective phase error* $e_{\Delta\psi_T,\alpha:\beta}$ in a $\alpha:\beta$ ratio-ed BLI. From (7), it is easy to see that

$$I_{\alpha,\beta} = \text{NINT}\left(R_{\alpha,\beta}\right) \quad \text{iff } |\Delta R_{\alpha,\beta}| < \frac{1}{2} \tag{8}$$

where NINT(x) equals to the nearest integer to x. In practice, we calculate $R_{\alpha,\beta}$ from practical phase measurement and then, using (8) which is known as the BLI *Characteristic Equation*, we compute $I_{\alpha,\beta}$ from $R_{\alpha,\beta}$. Equation (5) is a linear diophantine equation [13], [14] which is then solved by finding out an integer solution K_β so that $\alpha K_\beta - I_{\alpha,\beta}$ is divisible by β and then taking the quotient as K_α. According to the theory of linear diophantine equations [13], [14], as the greatest common divisor (GCD) of (α, β) equals unity, solutions to (5) exist and are given by a unique sequence of the form: $K_\alpha = k_\alpha \pm \alpha t$ and $K_\beta = k_\beta \pm \beta t$, where t is an integer and (k_α, k_β) are any particular solution for the given $I_{\alpha,\beta}$. In other words, in every range of size α, there exists exactly one solution of K_α and similarly, in every range of size β, there exists exactly one solution of K_β. Recalling that K_α and K_β restrict their values from 0 to $\alpha - 1$ and 0 to $\beta - 1$, respectively, for a given span of FOV$_T$, by restricting the solution for K_α to the range from 0 to $\alpha - 1$, one automatically obtains the solution for K_β in the range from 0 to $\beta - 1$. Substituting the solutions in (4a) and (4b), ambiguity in $\Delta\psi_\alpha$ and $\Delta\psi_\beta$ is then resolved.

B. Tolerable Phase Error Margin and Probability of Ambiguity

The *TPM* is a bound on phase measurement errors at individual antennas which guarantee zero ambiguity in differential phase measurements. From $|\Delta R_{\alpha,\beta}| < 1/2$ in (8) and the definition of $\Delta R_{\alpha,\beta}$, we note that a necessary and sufficient condition for zero ambiguity in differential phase measurements is given by

$$\left|\beta \cdot e_{\Delta\psi_\alpha} - \alpha \cdot e_{\Delta\psi_\beta}\right| < \pi. \tag{9}$$

In case of fixed three-element BLI configurations with inter-element ratio $m:n$, the total effective phase error is same for all three configurations, i.e., *mid-phase (MP)* with $m:n$ ratio-ed BLI, *end-phase left (EPL)* with $m:m+n$ ratio-ed BLI, and *end-phase right (EPR)* with $n:m+n$ ratio-ed BLI, as shown in [5] and [9]. Denoting by e_{ψ_i} the phase measurement error at the ith antenna (meaning, the differential phase error between the ith and jth antennas is given by $e_{\psi_i} - e_{\psi_j}$), (9) in this case turns out to be [5], [9]

$$|n \cdot e_{\psi_1} - (m+n) \cdot e_{\psi_2} + m \cdot e_{\psi_3}| < \pi. \tag{10}$$

We assume the same TPM, say, $e_{\psi,\text{TPM}}$ for each of $e_{\psi_1}, e_{\psi_2}, e_{\psi_3}$, i.e., $-e_{\psi,\text{TPM}} < e_{\psi_1}, e_{\psi_2}, e_{\psi_3} < +e_{\psi,\text{TPM}}$. To obtain a sufficient condition on $e_{\psi,\text{TPM}}$ for the satisfaction of (10), we consider the worst-case scenario: $e_{\psi_1} = e_{\psi_3} = +e_{\psi,\text{TPM}}$, $e_{\psi_2} = -e_{\psi,\text{TPM}}$. From (10), one then obtains the sufficient condition, $e_{\psi,\text{TPM}} = \frac{\pi}{2(m+n)}$. Considering the worst case again, the TPM $e_{\Delta\psi,\text{TPM}}$ for the differential phase error is then given by twice $e_{\psi,\text{TPM}}$, i.e.,

$$e_{\Delta\psi,\text{TPM}}\Big|_{FE} = \frac{\pi}{m+n}. \tag{11}$$

Here, suffix FE is used to indicate fixed-element BLI.

To derive the *probability of ambiguity* expression similar to [5] and [9], we assume that $e_{\Delta\psi_T,\alpha:\beta}$ follows the Gaussian distribution with zero mean and standard deviation $\sigma_{T,\alpha:\beta}$, where $\sigma^2_{T,\alpha:\beta} = E[(\beta e_{\Delta\psi_\alpha} - \alpha e_{\Delta\psi_\beta})^2]$. The differential phase errors $e_{\Delta\psi_\alpha}$ and $e_{\Delta\psi_\beta}$ are assumed to have the same variances, given by σ^2_{BL}. Defining the correlation coefficient $\rho_{\alpha:\beta} = \frac{E[e_{\Delta\psi_\alpha} \cdot e_{\Delta\psi_\beta}]}{\sigma^2_{BL}}$, we can then write $\sigma^2_{T,\alpha:\beta} = \sigma^2_{BL}[\alpha^2 + \beta^2 - 2\rho_{\alpha:\beta}\alpha\beta]$. From (9), the probability of correct ambiguity resolution P_c^π is given by the probability of $e_{\Delta\psi_T,\alpha:\beta}$ not exceeding $\pm\pi$, i.e., $P_c^\pi = \frac{1}{\sqrt{2\pi}\sigma_{T,\alpha:\beta}} \int_{-\pi}^{\pi} e^{-\frac{e^2_{\Delta\psi_T,\alpha:\beta}}{2\sigma^2_{T,\alpha:\beta}}} de_{\Delta\psi_T,\alpha:\beta}$. Equivalently, the probability of ambiguity P_a^π is given by

$$P_a^\pi = 1 - P_c^\pi = \text{erfc}\left(\frac{\pi}{\sqrt{2}\sigma_{BL}\sqrt{\alpha^2 + \beta^2 - 2\rho_{\alpha:\beta}\alpha\beta}}\right) \tag{12}$$

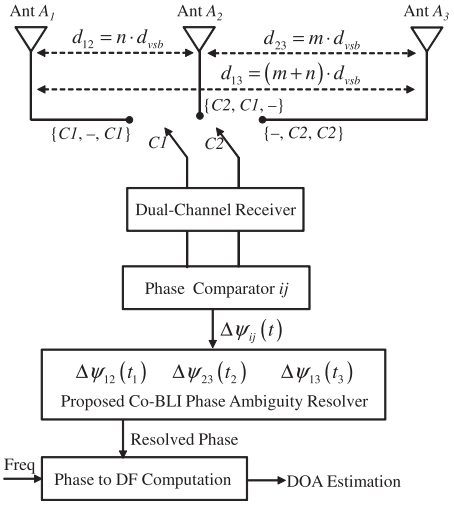

Fig. 2. Block diagram of a dual channel switched three-element BLI array.

where suffix π in P_a^{π} or P_c^{π} denotes that the boundary limit of $e_{\Delta\psi_T,\alpha:\beta}$ to avoid gross error in DOA caused by ambiguity is $\pm\pi$.

In a BLI configuration, as every pair of channels (say, ith and jth) are physically separated, we can assume their respective channel phase errors $e_{\psi_i}(t)$ and $e_{\psi_j}(t)$ at time t to be mutually uncorrelated, also having same variances σ^2, i.e., $E[e_{\psi_i}(t)e_{\psi_j}(t)] = \sigma^2\delta_{i,j}$. From $\sigma_{BL}^2 = E[(e_{\psi_i}(t) - e_{\psi_j}(t))^2]$, it then follows that $\sigma^2 = \frac{\sigma_{BL}^2}{2}$. For EPL array, the correlation coefficient $\rho_{m:m+n} = \frac{E[e_{\Delta\psi_m}(t)e_{\Delta\psi_{m+n}}(t)]}{\sigma_{BL,m}\sigma_{BL,m+n}} = \frac{E[(e_{\psi_1}(t)-e_{\psi_2}(t))(e_{\psi_1}(t)-e_{\psi_3}(t))]}{\sigma_{BL,m}\sigma_{BL,m+n}}$ or $\rho_{m:m+n} = \frac{E[e_{\psi_1}(t)e_{\psi_1}(t)]}{\sigma_{BL}^2} = \frac{\sigma^2}{\sigma_{BL}^2} = \frac{1}{2}$. In a similar manner, for MP and EPR arrays, $\rho_{m:n} = -\frac{1}{2}$ and $\rho_{n:m+n} = \frac{1}{2}$, respectively. Thus, irrespective of BLI ratio being $m : m+n$, $m : n$ or $n : m+n$, the total phase error variance remains the same, i.e., $\sigma_{T,m:m+n}^2 = \sigma_{T,m:n}^2 = \sigma_{T,n:m+n}^2$ which is given by $\sigma_{BL}^2(m^2 + n^2 + mn)$. Using this in (12), the probability of ambiguity for fixed-element BLI configuration [5] is then obtained as

$$P_{a,FE}^{\pi} = \text{erfc}\left(\frac{\pi}{\sqrt{2}\sigma_{BL}\sqrt{m^2+n^2+mn}}\right). \tag{13}$$

III. PROPOSED BLI ALGORITHM

A. SWaP Optimized ES onfiguration

In place of fixed-element receiver, we consider here a dual-channel switched receiver as a solution to SWaP optimized ES receiver configuration. The switched receiver is shown in Fig. 2, where switching takes place between a pair of antennas forming various baselines. The differential phase measurement errors amongst the pair of baselines may not be correlated now as differential phases from baselines are sampled at different time instants (t, t'). Similar situations also arise in applications [15] where the baselines are formed using all different antennas due to space constraints.

In case of a switched three-element MP array for $m : n$ ratio-ed BLI, $e_{\Delta\psi,m:n} = n \cdot e_{\Delta\psi_m}(t) - m \cdot e_{\Delta\psi_n}(t') = n \cdot (e_{\psi_1}(t) - e_{\psi_2}(t)) - m \cdot (e_{\psi_2}(t') - e_{\psi_3}(t'))$. Using the similar logic, as used in Section II-B, a sufficient condition to ensure $|e_{\Delta\psi,m:n}| < \pi$ is obtained by considering the worst-case scenario: $e_{\psi_1}(t) = e_{\psi_3}(t') = +e_{\psi,\text{TPM}}$, $e_{\psi_2}(t) = e_{\psi_2}(t') = -e_{\psi,\text{TPM}}$. For the differential phase error, this leads to

$$e_{\Delta\psi,\text{TPM}}\Big|_{m:n,SE} = \frac{\pi}{m+n}. \tag{14}$$

Similarly, for EPL- and EPR-array

$$e_{\Delta\psi,\text{TPM}}\Big|_{m:m+n,SE} = \frac{\pi}{2m+n} \tag{15a}$$

$$\text{and, } e_{\Delta\psi,\text{TPM}}\Big|_{n:m+n,SE} = \frac{\pi}{m+2n}. \tag{15b}$$

respectively (the suffix SE is used to indicate switched-element BLI). Now, we will derive probability of ambiguity expression for dual channel switched-configuration. Unlike the fixed-element case, in the case of switched-element case $E[e_{\psi_i(t)}e_{\psi_i(t')}] \neq \sigma^2$ and equals to zero if sampling instant t and t' are well separated. Hence, $\rho_{m:m+n} = \rho_{m:n} = \rho_{n:m+n} = 0$, and thus, from above

$$P_{a,m:n,SE}^{\pi} = \text{erfc}\left(\frac{\pi}{\sqrt{2}\sigma_{BL}\sqrt{m^2+n^2}}\right), \tag{16a}$$

$$P_{a,m:m+n,SE}^{\pi} = \text{erfc}\left(\frac{\pi}{\sqrt{2}\sigma_{BL}\sqrt{m^2+(m+n)^2}}\right), \tag{16b}$$

$$P_{a,n:m+n,SE}^{\pi} = \text{erfc}\left(\frac{\pi}{\sqrt{2}\sigma_{BL}\sqrt{n^2+(m+n)^2}}\right). \tag{16c}$$

We observe from above that $P_{a,m:n,SE}^{\pi} < P_{a,m:m+n,SE}^{\pi} < P_{a,n:m+n,SE}^{\pi}$ because $0 < m < n$. Thus, the $m:n$ array has minimum probability of ambiguity though it does not offer minimum DOA estimate error, whereas $m : m+n$ or $n:m+n$ array provides minimum DOA estimation error but has probability of ambiguity higher than the $m:n$ array. This has given a motivation to develop a new approach toward the design of a three-element BLI array which retains the minimum probability of ambiguity of the $m:n$ configuration, while achieving the maximum DOA accuracy, as obtained in the $m : m+n$ or $n:m+n$ array.

B. Cooperative BLI (Co-BLI) Triplet

THEOREM 1: In a three-antenna, switched BLI array with inter-element spacings md_{vsb} and nd_{vsb}, m and n being coprime and $0 < m < n$, if ARNs of $(m:n)$ and $(n:m+n)$ ratio-ed BLI are jointly observed, it is possible to resolve the phase ambiguity in the longest baseline $(m+n)d_{vsb}$ while achieving TPM at least equal to $\frac{\pi}{m+n}$ (i.e., maximum obtainable individually by the $(m:n)$, $(m : m+n)$ and $(n:m+n)$ ratio-ed BLI).

PROOF: Consider the *switched-element* case, as shown in Fig. 2. The three measured differential phases are obtained in three different time-instants. For simplification of notation, we denote $\Delta\psi_{12}(t_1)$ as $\Delta\psi_m$, $\Delta\psi_{23}(t_2)$ as

$\Delta\psi_n$ and $\Delta\psi_{13}(t_3)$ as $\Delta\psi_{m+n}$. First assume that for the $m{:}n$ array, the sufficient condition that the differential phase error lies within $\pm\frac{\pi}{m+n}$ is satisfied, meaning, from (14), $I_{m,n}$ and thereby, K_m and K_n are available correctly. Next, for the $n{:}m+n$ ratio, from (7) and (5), we can write, $R_{n,m+n} = (nK_{m+n} - (m+n)K_n) + \Delta R_{n,m+n}$, where $\Delta R_{n,m+n} = \frac{(m+n)e_{\Delta\psi_n} - ne_{\Delta\psi_{m+n}}}{2\pi}$. Since the value of K_n is correctly known, this can be rewritten as

$$\frac{R_{n,m+n} + (m+n)K_n}{n} = K_{m+n} + \frac{\Delta R_{n,m+n}}{n}.$$

Following the lines of (8) and (9), we can then write,

$$K_{m+n} = \text{NINT}\left(\frac{R_{n,m+n} + (m+n)K_n}{n}\right)$$

$$\text{iff } \left|\Delta R_{n,m+n}\right| < \frac{n}{2}, \text{ i.e., } \left|e_{\Delta\psi_{T,n:m+n}}\right| < n\pi. \tag{17}$$

Simplifying, we obtain a new tolerable limit for the differential-phase error as $\frac{\pi n}{m+2n}$, which is easily seen to be higher than $\frac{\pi}{m+n}$ for $n \geqslant 2$. Since $0 < m < n$, we always have $n \geqslant 2$, meaning $\frac{\pi n}{m+2n} > \frac{\pi}{m+n}$ for all values of m and n. Since the antennas are common for both the $(m{:}n)$ and $(n{:}m+n)$ ratio-ed BLIs, a sufficient condition (though not necessary) for resolution of phase ambiguity in the longest baseline $(m+n)d_{\text{vsb}}$ is obtained by taking the lower of the two figures, $\frac{\pi n}{m+2n}$, $\frac{\pi}{m+n}$ which is $\frac{\pi}{m+n}$. Hence proved. ■

Observations:

1) Similar logic as above, when applied to the co-operative pair $(m{:}n, m{:}m+n)$, results in a TPM of $\frac{\pi m}{2m+n}$ for the longest baseline $(m+n)d_{\text{vsb}}$. It is, however, seen that $\frac{\pi m}{2m+n} > \frac{\pi}{m+n}$ for $m \geq 2$, i.e., *not* for all values of m, n. Hence, we will consider $(m{:}n, n{:}m+n)$ to be the default cooperative pair (unless otherwise stated) and shall denote it simply by $(m{:}n{:}m+n)$.
2) The overall probability of ambiguity for SE co-operative pair $(m{:}n, n{:}m+n)$ is $P^{\pi,n\pi}_{a,m:n,n:m+n,SE} = 1 - P\left(\left|e_{\Delta\psi_{T,n:m+n}}\right| < n\pi \cap \left|e_{\Delta\psi_{T,m:n}}\right| < \pi\right)$.

COROLLARY: In case of SE configuration, the probability of ambiguity of the Co-BLI algorithm is almost at par with the normal $m{:}n$ BLI algorithm at high SNR (e.g., 10 dB or above).

PROOF: Under high SNR, the event $\left|e_{\Delta\psi_{T,n:m+n}}\right| < n\pi$, under the condition $\left|e_{\Delta\psi_{T,m:n}}\right| < \pi$ has a probability almost one, and thus, the joint probability $P\left(\left|e_{\Delta\psi_{T,n:m+n}}\right| < n\pi \cap \left|e_{\Delta\psi_{T,m:n}}\right| < \pi\right) \approx P\left(\left|e_{\Delta\psi_{T,m:n}}\right| < \pi\right)$. As a result, $P^{\pi,n\pi}_{a,m:n:m+n,SE}\big|_{\text{high SNR}} \approx P^{\pi}_{a,m:n,SE}$.

The basic Co-BLI algorithm discussed above, is based on a three-antenna array, thus the name "triplet." Next, we will extend to a four-antenna array and then generalize to $(p+2)$-antenna array to achieve further more DF accuracy. ■

C. Extension of Co-BLI Triplet for Four or More Antenna BLI Array

Since longer the baseline distances, more accurate are the DF estimates, as discussed in Section II, we use a positive integer factor δ to have increased inter-element spacings as $m\delta.d_{\text{vsb}}$ and $n\delta.d_{\text{vsb}}$ maintaining the $m{:}n$ ratio in the three-antenna BLI array. Here, similar to (4), we can write

$$\Delta\psi_{m\delta} = \Delta\psi^T_{m\delta} + e_{\Delta\psi_{m\delta}} - 2\pi K_{m\delta}, \tag{18a}$$

$$\Delta\psi_{n\delta} = \Delta\psi^T_{n\delta} + e_{\Delta\psi_{n\delta}} - 2\pi K_{n\delta}, \tag{18b}$$

where $K_{m\delta}$ and $K_{n\delta}$ assume positive integer values from 0 to $m\delta - 1$ and 0 to $n\delta - 1$, respectively, as from (1) and from the definition of d_{vsb}, the ranges of $\Delta\psi^T_{m\delta}$ and $\Delta\psi^T_{n\delta}$ are now $[0, 2\pi m\delta]$ and $[0, 2\pi n\delta]$, respectively. We first divide the range 0 to $m\delta - 1$ of $K_{m\delta}$ into δ sub-blocks of length m each, with the lth sub-blocks, $0 \leq l \leq \delta - 1$, given by indices from lm to $lm + m - 1$. Then, any $K_{m\delta}$ in the above range can be expressed as $K_{m\delta} = K^{\delta}_m + mK_{\delta}$, where $0 \leq K^{\delta}_m \leq m - 1$ and $0 \leq K_{\delta} \leq \delta - 1$ (i.e., K_{δ} and K^{δ}_m are the quotient and remainder, respectively, obtained by division of $K_{m\delta}$ by m). Substituting in (18a) and recalling that $\Delta\psi^T_{m\delta} = \frac{2\pi}{\lambda}\, m\delta d_{\text{vsb}} \sin\theta$, we obtain, from (18a),

$$\frac{\delta\, d_{\text{vsb}}\sin\theta}{\lambda} = \frac{\Delta\psi_{m\delta} - e_{\Delta\psi_{m\delta}} + 2\pi K^{\delta}_m}{2\pi m} + K_{\delta}. \tag{19}$$

Under high SNR condition, $\Delta\psi_{m\delta} - e_{\Delta\psi_{m\delta}}$ $(= \Delta\psi^T_{m\delta} - 2\pi K_{m\delta})$ lies between zero and 2π. From this and the fact that $0 \leq K^{\delta}_m \leq m - 1$, it follows that the first term on the RHS of (19) is a fraction (< 1), meaning that K_{δ} in (19) is the integer part in the division of $\delta\, d_{\text{vsb}}\sin\theta$ by λ. This shows that K_{δ} is independent of m, i.e., its value does not change if m is replaced by n. Following similar arguments, we can then express $K_{n\delta}$ in (18b) as $K_{n\delta} = K^{\delta}_n + nK_{\delta}$, where $0 \leq K^{\delta}_n \leq n - 1$. Defining $\Delta\widetilde{\psi}^T_{m\delta} = \Delta\psi^T_{m\delta} - 2\pi mK_{\delta}$ and $\Delta\widetilde{\psi}^T_{n\delta} = \Delta\psi^T_{n\delta} - 2\pi nK_{\delta}$ with respective ranges of $[0, 2\pi m]$ and $[0, 2\pi n]$, we rewrite (18) as

$$\Delta\psi_{m\delta} = \Delta\widetilde{\psi}^T_{m\delta} + e_{\Delta\psi_{m\delta}} - 2\pi K^{\delta}_m, \tag{20a}$$

$$\Delta\psi_{n\delta} = \Delta\widetilde{\psi}^T_{n\delta} + e_{\Delta\psi_{n\delta}} - 2\pi K^{\delta}_n. \tag{20b}$$

Since $n\Delta\widetilde{\psi}^T_{m\delta} - m\Delta\widetilde{\psi}^T_{n\delta} = 0$ (as K_{δ} is common between $\Delta\widetilde{\psi}^T_{m\delta}$ and $\Delta\widetilde{\psi}^T_{n\delta}$), we can follow steps similar to as has been used to obtain (7) and (8) from (4), resulting in the diophantine equation $I_{m,n} = mK^{\delta}_n - nK^{\delta}_m$ whose solution gives us K^{δ}_m and K^{δ}_n. By similar logic, we can extend this to the Co-BLI triplet $m{:}n{:}m+n$ for higher DF accuracy resulting in K^{δ}_{m+n} for the longest baseline $(m+n)\cdot\delta\cdot d_{\text{vsb}}$. This array is termed as the Co-BLI array$-\delta$. However, unlike earlier in Section II, ambiguities in $\Delta\psi_{m\delta}$ and $\Delta\psi_{n\delta}$ ($\Delta\psi_{(m+n)\delta}$ in case of the Co-BLI) are still not totally resolved because the value of K_{δ} is not known yet.

In order to resolve the residual ambiguities in $\Delta\psi_{(m+n)\delta}$ by obtaining the K_{δ} value, we introduce another three-antenna array (say, Co-BLI array$-\gamma$), obtained by increasing the inter-element spacings by a positive integer

γ which is coprime with δ and also, $0 < \delta < \gamma$, giving rise to inter-element distances $m\gamma.d_{\text{vsb}}$ and $n\gamma.d_{\text{vsb}}$. Now we apply $m{:}n{:}m+n$ Co-BLI triplet taking inter-element distance ratio $m{:}n$ in Co-BLI array $-\delta$ and $-\gamma$. We resolve partial ambiguities, as discussed above, in respective Co-BLI arrays corresponding to their longest baselines $(m+n)\cdot\delta\cdot d_{\text{vsb}}$ and $(m+n)\cdot\gamma\cdot d_{\text{vsb}}$ by obtaining values of K^{δ}_{m+n} and K^{γ}_{m+n}. Once the values are obtained, we compute $\Delta\widetilde{\psi}_{(m+n)\delta} = \Delta\psi_{(m+n)\delta} + 2\pi K^{\delta}_{m+n}$ and $\Delta\widetilde{\psi}_{(m+n)\gamma} = \Delta\psi_{(m+n)\gamma} + 2\pi K^{\gamma}_{m+n}$. Till this, we call it the first level of the Co-BLI ambiguity resolver, where phases corresponding to the longest baseline in both the arrays are partially resolved up to $2(m+n)\pi$. As before, the first-level (Co-BLI) can achieve TPM as $e_{\Delta\psi_{L1,\text{TPM}}} = \frac{\pi}{m+n}$. Now, in the second level, we further resolve ambiguity corresponding to the longest baseline in $\Delta\widetilde{\psi}_{(m+n)\gamma}$ by determining the value of K_{γ} as a solution of the following $\delta:\gamma$ ratio-ed BLI equations:

$$\Delta\widetilde{\psi}_{(m+n)\delta} = \Delta\psi^{T}_{(m+n)\delta} + e_{\Delta\psi_{(m+n)\delta}} - 2\pi(m+n)K_{\delta}, \quad (21a)$$

$$\Delta\widetilde{\psi}_{(m+n)\gamma} = \Delta\psi^{T}_{(m+n)\gamma} + e_{\Delta\psi_{(m+n)\gamma}} - 2\pi(m+n)K_{\gamma}. \quad (21b)$$

Equation (21) can be solved and K_{γ}, K_{δ} can be obtained, by first dividing both sides of (21a) and (21b) by $(m+n)$ and then applying the normal BLI technique similar to as used in obtaining (7) and (8) from (4), i.e., by multiplying both sides of (21a) by γ and of (21b) by δ, and subtracting latter from the former. Proceeding along similar lines, it is easy to see that the TPM in the second level is given by $e_{\Delta\psi_{L2,\text{TPM}}} = \frac{\pi(m+n)}{\delta+\gamma}$. This implies that the phase ambiguity in $\Delta\widetilde{\psi}_{(m+n)\gamma}$ is resolved up to $2(m+n)\gamma\pi$ provided the phase error is within its TPM $e_{\Delta\psi_{L2,\text{TPM}}}$, and further, DOA can be estimated without any ambiguities from the fully resolved $\Delta\widetilde{\psi}_{(m+n)\gamma}$ corresponding to the longest baseline $(m+n)\gamma.d_{\text{vsb}}$. However, as this assumes successful partial ambiguity resolution in the first level, the overall TPM cannot exceed $e_{\Delta\psi_{L1,\text{TPM}}}$. Therefore, to ensure that the overall TPM can be taken as $e_{\Delta\psi_{L1,\text{TPM}}} = \frac{\pi}{m+n}$, we need to maintain $e_{\Delta\psi_{L1,\text{TPM}}} \leqslant e_{\Delta\psi_{L2,\text{TPM}}}$, i.e., $(\delta+\gamma) \leqslant (m+n)^2$.

Antenna Selection: In general, five antennas (two sets of three antennas with one common) are required for any value of δ and γ. To optimize the same with the four-antenna array, there should be one common inter-element spacing in Co-BLI array-δ and array-γ. For that, (δ, γ) may be equated to three possible sets of values as follows.

(A) $\delta = m,\ \gamma = n$, resulting in two arrays, $m^2{:}mn$ and $mn{:}n^2$ from which the segment mn can be taken as common, giving rise to the four-element array $m^2{:}\,mn{:}\,n^2$.

(B) $\delta = m,\ \gamma = m+n$, resulting in two arrays, $m^2{:}mn$ and $m(m+n){:}n(m+n)$, out of which we take the segment $m(m+n)$ common (for the δ-array, it is the longest inter-element segment), resulting in the four-element array $m^2{:}\,mn{:}n(m+n)$.

(C) $\delta = n,\ \gamma = m+n$, resulting in the four-element array $mn{:}n^2{:}m(m+n)$ or equivalently, $n^2{:}\,mn{:}m(m+n)$ by similar reasoning. This is illustrated in Fig. 3.

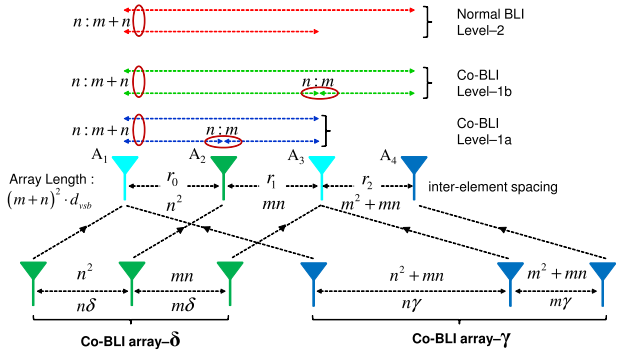

Fig. 3. Formation of four-element second-order Co-BLI array for $\gamma:\delta = m+n{:}n$. Same can be drawn for $\gamma:\delta = m+n{:}m$ in a similar way.

It is easy to check that all the above choices of δ, γ satisfy the following: (i) $\delta < \gamma$, (ii) $\delta+\gamma < (m+n)^2$, and (iii) δ, γ are coprime. Of these, the choice under (A) above is suboptimal since it considers $n(n+m).d_{\text{vsb}}$ and not the end-to-end element spacing $(n^2+mn+m^2).d_{\text{vsb}}$ as the longest baseline in the four-antenna array. Hence, $m^2{:}mn{:}n(m+n)$ and $n^2{:}nm{:}m(n+m)$ are treated as the four-antenna Co-BLI array with end-to-end element spacing $(m+n)^2 d_{\text{vsb}}$, thus implying it is a second-order Co-BLI. The condition $\delta+\gamma < (m+n)^2$, however, puts a constraint on the maximum values that can be chosen for δ, γ, and thus, constrains the maximum accuracy achievable in the DOA. To overcome this problem, we extend the four-antenna BLI to a five-antenna-based one and further using the same philosophy as was used to extend the three-antenna to the four-antenna BLI and is discussed as follows.

Further Extensions: To extend the accuracy further, we increase the inter-element spacing of an $m\delta:n\delta$ array by an integer, say, μ, meaning, like (18a) and (18b), we will have, (i) $\Delta\psi_{m\delta\mu} = \Delta\psi^{T}_{m\delta\mu} + e_{\Delta\psi_{m\delta\mu}} - 2\pi K_{m\delta\mu}$, and (ii) $\Delta\psi_{n\delta\mu} = \Delta\psi^{T}_{n\delta\mu} + e_{\Delta\psi_{n\delta\mu}} - 2\pi K_{n\delta\mu}$, where $0 < \Delta\psi_{m\delta\mu},\ \Delta\psi_{n\delta\mu} < 2\pi$, $0 < \Delta\psi^{T}_{m\delta\mu} < 2\pi m\delta\mu$, $0 < \Delta\psi^{T}_{n\delta\mu} < 2\pi n\delta\mu$, $0 < K_{m\delta\mu} < m\delta\mu - 1$, and $0 < K_{n\delta\mu} < n\delta\mu - 1$. For $K_{m\delta\mu}$, we divide the range $0-(m\delta\mu-1)$ in μ blocks of length δm each and then each such block is divided into δ sub-blocks of length m each, whereby $K_{m\delta\mu}$ is expressed as $K_{m\delta\mu} = K^{\delta\mu}_{m} + m(K^{\mu}_{\delta} + \delta K_{\mu})$, where, $0 \le K^{\delta\mu}_{m} \le m-1, 0 \le K^{\mu}_{\delta} \le \delta - 1$ and $0 \le K_{\mu} \le \mu - 1$. Substituting in (i), it is seen that $K^{\mu}_{\delta} + \delta K_{\mu}$ is the integer part in the division $\frac{\mu\delta.d_{\text{vsb}}.\sin\theta}{\lambda}$ and is thus independent of m. Similarly, we define $K_{n\delta\mu} = K^{\delta\mu}_{n} + n(K^{\mu}_{\delta} + \delta K_{\mu})$, where $0 \le K^{\delta\mu}_{n} \le n-1$. Then, following identical steps as used earlier (i.e., level-1), we first solve for $K^{\delta\mu}_{m}$ and $K^{\delta\mu}_{n}$ followed by $K^{\delta\mu}_{m+n}$ (i.e., extending it to $m{:}n{:}m+n$ Co-BLI triplet). Then, using another $m\gamma:n\gamma$ array, we determine K^{μ}_{δ} and K^{μ}_{γ} (i.e., level-2), which leaves K_{μ} as the only unknown left out. To solve for it, we deploy another four-antenna array by replacing μ by ν which are mutually coprime ($\mu < \nu$) and carry out the same steps, resulting in a single unknown term K_{ν}. The two terms K_{μ} and K_{ν} from the two arrays are then solved and the ambiguity is fully resolved. The last step constitutes level-3.

Using same steps as used earlier, it is easy to check that the TPM for level-3 will be $e_{\Delta\psi_{L3,\mathrm{TPM}}} = \frac{\pi(m+n)\gamma}{\mu+\nu}$, and to ensure that $e_{\Delta\psi_{L3,\mathrm{TPM}}} \le e_{\Delta\psi_{L1,\mathrm{TPM}}}$ so that overall TPM remains $e_{\Delta\psi_{L1,\mathrm{TPM}}}$, we need to have $(\mu+\nu) \le (m+n)^2\gamma$. Also, the level-3 will resolve ambiguity upto $2\pi(m+n)\gamma\nu$. To state the general result which follows easily from above, we now make a slight change in the notations. We, respectively, denote δ and γ by δ_1 and γ_1, μ and ν by δ_2 and γ_2, and in general, denote by δ_p and γ_p ($\delta_p < \gamma_p$, δ_p and γ_p are coprime) the constants used to multiply the inter-element spacings of the existing array at the $(p+1)$th level ($p \ge 1$). Then, from above, the following general results can be stated: for level-1, the maximum resolvable ambiguity is $2\pi(m+n)$, and for any $(p+1)$th level, $p \ge 1$, it is $2\pi(m+n)\prod_{i=1}^{p}\gamma_i$. Further, such ambiguity resolution will require satisfaction of the following inequalities: $(\delta_1+\gamma_1) \le (m+n)^2$ for level-2 and $(\delta_i+\gamma_i) \le (m+n)^2\prod_{j=1}^{i-1}\gamma_j$, $i = 2, 3, \ldots, p$, for level $(p+1)$.

As in the case of level-2, for level-3 also, the number of antenna elements can be optimized provided we take $\delta_1 = \delta_2$ ($= m$ or n) and $\gamma_1 = \gamma_2$ ($= m+n$). For $\delta_1 = \delta_2 = m$, starting from the four-element array $m^2 : mn : n(m+n)$, we have the two arrays: $m^3 : m^2n : (m+n)mn$ and $m^2(m+n) : (m+n)mn : (m+n)^2n$, out of which we take the two segments $m^3 : m^2$ ($\equiv m^2(m+n)$) and $(m+n)mn$ as common, resulting in the five-element array $m^3 : m^2n : (m+n)mn : (m+n)^2n$. In a similar manner, for $\delta_1 = \delta_2 = n$ and starting from $n^2 : mn : m(m+n)$, we will have $n^3 : n^2\,m : (m+n)mn : (m+n)^2\,m$. From this, it is possible to state the following general result: for the pth level ($p \ge 1$), the array will have $(p+2)$ antennas or, equivalently, $(p+1)$ inter-antenna segments, where the ith segment (normalized to d_{vsb}) r_i, $i = 0, 1, \ldots, p$ between the antennas A_{i+1} and A_{i+2} is given as

$$r_i = \begin{cases} n^p, & i = 0 \\ n^{p-i}m(m+n)^{i-1}, & i = 1, 2, \ldots, p \end{cases} \tag{22a}$$

$$\text{or,} \quad \begin{cases} m^p, & i = 0 \\ m^{p-i}n(n+m)^{i-1}, & i = 1, 2, \ldots, p. \end{cases} \tag{22b}$$

In the above, (22a) corresponds to $\delta_i = n$, $\gamma_i = (m+n)$ and (22b) corresponds to $\delta_i = m$, $\gamma_i = (m+n)$. This type of array can be termed as the pth-order BLI array due to fact that the total distance between end-to-end element is $(m+n)^p.d_{\mathrm{vsb}}$. The consecutive inter-element spacings in (22b) are in increasing order with least value $m^p.d_{\mathrm{vsb}}$ as $m < n$ which is usually much less than the minimum inter-element spacing in (22a). Sometimes due to large aperture size, antennas covering wide-band (say, 2–18 GHz) do not fit in the least inter-element spacing $m^p.d_{\mathrm{vsb}}$. Due to this, the Co-BLI array in (22a) may be more appropriate for use in practice. In either case, the $m:n:m+n$ Co-BLI can be applied for p number of antenna-triplets between baselines, containing $(A_1 - A_2 - A_3)$, $(A_1 - A_3 - A_4)$,..., $(A_1 - A_{l-1} - A_l)$,..., $(A_1 - A_{p+1} - A_{p+2})$ in the first level, as shown in Fig. 4. Then, normal BLI is applied to $(p-1)$ number of $m:m+n$ or $n:n+m$ ratio-ed antenna arrays in the second level, $(p-2)$ antenna arrays in the third level, and so on and so forth, finally to one $m:m+n$ or $n:n+m$ ratio-ed antenna array ratio, at the pth level.

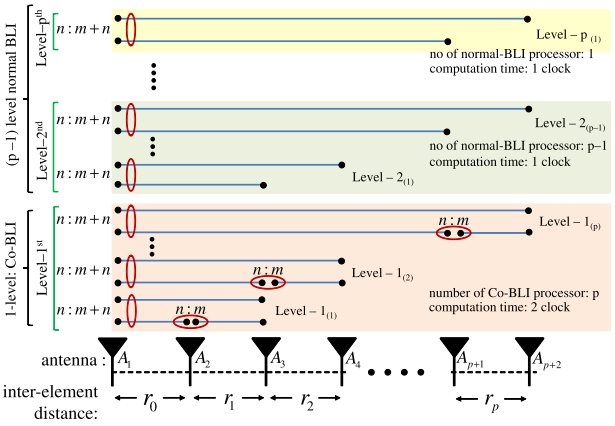

Fig. 4. Generalized pth-order Co-BLI array having $(p+2)$-antennas with p-level processing for $\gamma : \delta = m+n : n$.

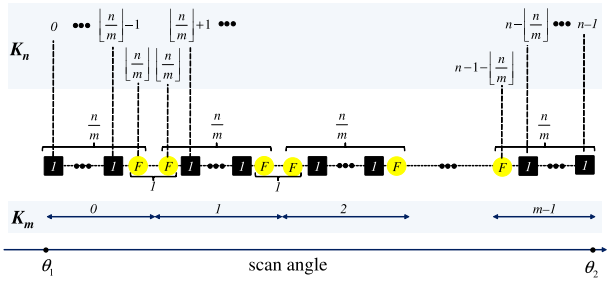

Fig. 5. 2π −cycle (1: full and F: fraction) flow for K_m and K_n in $m:n$ ratio-ed BLI.

IV. IMPLEMENTATION ISSUES

In a practical implementation of the proposed scheme, the primary computational task is to solve the linear diophantine (5) for various values of m and n depending on the level of the Co-BLI ambiguity resolver. While $0 \le K_m \le m-1$ and $0 \le K_n \le n-1$, it may be noted that all the mn combinations of K_m and K_n do not, however, arise in practice, since, in both $\Delta\psi_m^T$ and $\Delta\psi_n^T$, the angle θ is common (in fact, $\frac{\Delta\psi_m^T}{\Delta\psi_n^T} = \frac{m}{n}$). To explain it in detail, assume that both K_m and K_n start at zero values at an angle $\theta = \theta_1$ and over a period θ_1-to-$\theta_1 + \Delta_\theta$, K_m remains zero (i.e., $\Delta\psi_m^T$ does not cross 2π). Also, for ease of explanation, we may assume Δ_θ to be small, and thus, $\sin\Delta_\theta \approx \Delta_\theta$. Then, for every increase of θ by $\frac{m}{n}\Delta_\theta$, the value of K_n increases by one while K_m remains constant at zero and this goes on till an angle $\theta = \lfloor\frac{n}{m}\rfloor\frac{m}{n}\Delta_\theta$ is covered beyond which K_n increases by one while K_m makes a transition from zero to one and this process again goes on. This is shown in Fig. 5. The above defines the permissible values of K_m and K_n and for each pair, the corresponding $I_{m,n}$ can be precomputed and stored. Since only a fraction of the total mn combinations come into play, storage space requirement is very much manageable. Note that as per this, given $R_{m,n}$, one has to first compute $I_{m,n}$ using (8) and then, from $I_{m,n}$, identify K_m, K_n

TABLE I
Mapping-Based Co-Operative Ambiguity Table (M-CAT) for 2 : 3 : 5 Co-BLI

Ranges of R_{35}	Ranges of R_{23}	K_5
-2 ± 1.5 (-3.5 to -0.5)	$+2 \pm 0.5$ ($+1.5$ to $+2.5$)	$+1$
-1 ± 1.5 (-2.5 to $+0.5$)	$+1 \pm 0.5$ ($+0.5$ to $+1.5$)	$+3$
0 ± 1.5 (-1.5 to $+1.5$)	0 ± 0.5 (-0.5 to $+0.5$)	0
$+1 \pm 1.5$ (-0.5 to $+2.5$)	-1 ± 0.5 (-1.5 to -0.5)	$+2$
$+1 \pm 1.5$ (-0.5 to $+2.5$)	$+2 \pm 0.5$ ($+1.5$ to $+2.5$)	$+2$
$+2 \pm 1.5$ ($+0.5$ to $+3.5$)	$+1 \pm 0.5$ ($+0.5$ to $+1.5$)	$+4$
$+3 \pm 1.5$ ($+1.5$ to $+4.5$)	0 ± 0.5 (-0.5 to $+0.5$)	$+1$
$+4 \pm 1.5$ ($+2.5$ to $+5.5$)	-1 ± 0.5 (-1.5 to -0.5)	$+3$

from the look-up-table. The computation of $I_{m,n}$ can be further avoided by noting from (7) that under the condition $|\Delta R_{m,n}| < 1/2$, range of $R_{m,n}$ is given by $I_{m,n} \pm 1/2$ and one thus can store the applicable ranges of $R_{m,n}$ as given by valid $I_{m,n}$ values, rather than $I_{m,n}$ itself. For a given $R_{m,n}$, the look-up-table will then directly give K_m and K_n.

This approach can now be extended to the Co-BLI as follows: first, like above, for every slot of the angle over which K_n remains fixed, K_{m+n} increases in steps of one which provide us valid values of K_n, K_{m+n}, and thus, of $I_{n,m+n} = nK_{m+n} - (m+n)K_n$. Recalling from Section III-B that $R_{n,m+n} = (nK_{m+n} - (m+n)K_n) + \Delta R_{n,m+n} \equiv I_{n,m+n} + \Delta R_{n,m+n}$, if, like in BLI, we assume $|\Delta R_{n,m+n}| < 1/2$, then, since for any pair of values, say, r and l of the API $I_{n,m+n}$, the ranges $r \pm 1/2$ and $l \pm 1/2$ do not overlap, each measured $R_{n,m+n}$ points to a $I_{n,m+n}$, or, equivalently to a pair K_{m+n}, K_n *uniquely*. However, as stated earlier, in Co-BLI, we take $|\Delta R_{n,m+n}| < n/2$. Clearly, there exist several values of $I_{n,m+n}$ in this case for which the ranges $I_{n,m+n} \pm n/2$ will overlap. However, as seen from (17), if the knowledge of K_n is available, then, even under $|\Delta R_{n,m+n}| < n/2$, one can obtain K_{m+n} (and thus, $I_{n,m+n}$) uniquely. In other words, while the ranges $I_{n,m+n} \pm n/2$ overlap for several values of $I_{n,m+n}$, each such overlapping region will have a distinct K_n and the measured $R_{n,m+n}$ together with K_n will point to the correct $I_{n,m+n}$ (or, equivalently, correct K_{m+n}). Since, as seen earlier, K_n has a one-to-one correspondence with $R_{m,n}$, the above amounts to storing ranges of $R_{n,m+n}$ (i.e., $I_{n,m+n} \pm \frac{n}{2}$) against ranges of applicable $R_{m,n}$ (i.e., $I_{m,n} \pm 1/2$) and corresponding K_{m+n}. The table where all such ranges of $R_{n,m+n}$, $R_{m,n}$, and K_{m+n} are stored is termed here as mapping-based cooperative ambiguity table (M-CAT). For the sake of an example, we show the M-CAT table for a Co-BLI ratio 2:3:5 in Table I, formed by computing and storing all applicable ranges.

V. SIMULATION AND FPGA BASED HARDWARE IMPLEMENTATION

The performance of the Co-BLI triplet is validated and compared with normal BLI through MATLAB simulation. We simulate a three-element Co-BLI array ($m:n:m+n$) and compare its performance with MP ($m:n$), EPL ($m:m+n$), and EPR ($n:m+n$) for an overall array length of ($m+n$) normalized to d_{vsb}. Of the various combinations of $m:n$ ratio possible for a constant $m+n$, we choose the one that has m/n ratio close to 1 so that the total array length is divided almost equally to accommodate large aperture antenna elements. For example, in case of total array length $m+n=7$, possible $m:n$ ratios are 1:6, 2:5, and 3:4; however, 3:4 is considered here as it can fit antenna having maximum diameter of $3d_{\text{vsb}}$. Following (1), we choose $d_{\text{vsb}} = 32$ mm to have minimum FOV$_T$ of 100° (±50°) at its highest frequency of operation in a 2–6 GHz Co-BLI array. Without loss of generality, the operating frequency is set to 6 GHz for simulation. We add zero-mean additive white Gaussian phase error having standard deviation (σ_{BL}) of 18° to the true differential phases at different time instants. This is equivalent to a 10 dB SNR condition [3]. Also, initially we take the total array length $m+n=3$ (norm. to d_{vsb}), i.e., 96 mm with minimum inter-element spacing as 32 mm. We apply Co-BLI and calculate DOA error at each angle at a step of 0.1° for a span from −45° to +45° keeping a margin of 5° on either side of the FOV$_T$. If any angle is having gross DOA estimation error, it is termed as an ambiguous point. We find out the probability of ambiguity P_a in each run spanning FOV$_T$ by calculating the number of ambiguous points normalized to total number of points. Overall P_a for a particular array length ($m+n$) is then taken as the average of 400 such independent runs. The same experiment is then repeated for increasing values of ($m+n$), from 4 to 25 to see how P_a changes with increase in the array length and the corresponding results are plotted in Fig. 6, both for the proposed Co-BLI and various BLI configurations like EPL, EPR, and MP, which clearly shows that the proposed Co-BLI has the least P_a at any array length, matching that of the MP array. The Co-BLI array, however, provides better DOA accuracy than the MP array as the latter does not utilize the total array length for DOA estimation. In the same figure, we also plot the theoretical values of P_a, as given by the expressions derived in the Section III. It shows that the simulation results are in good agreement with the theoretical ones. Next, we keep the total array length $m+n$ fixed at 5 and plot P_a against increasing σ_{BL} (or equivalently,

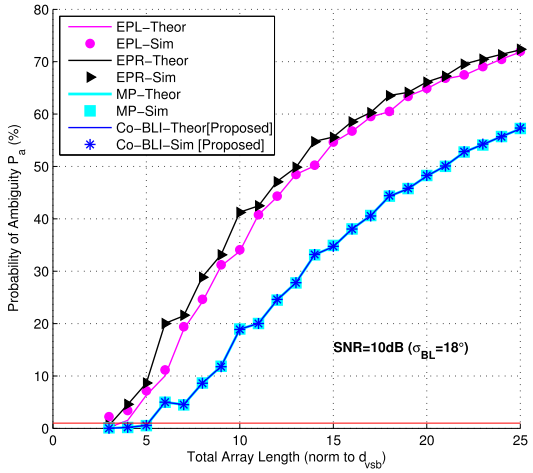

Fig. 6. Performance comparison of three-element Co-BLI with EPL, EPR, and MP BLI arrays: probability of ambiguity $P_a(\%)$ versus total array length (norm to d_{vsb}). [legend: -Theor: theoretical; -Sim: simulation].

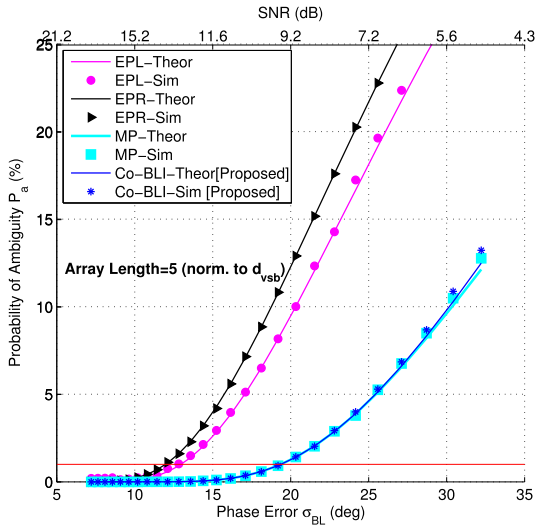

Fig. 7. Performance comparison of three-element Co-BLI with EPL, EPR, and MP BLI arrays: probability of ambiguity $P_a(\%)$ versus phase error σ_{BL} and SNR_{dB}.[legend: -Theor: theoretical; -Sim: simulation].

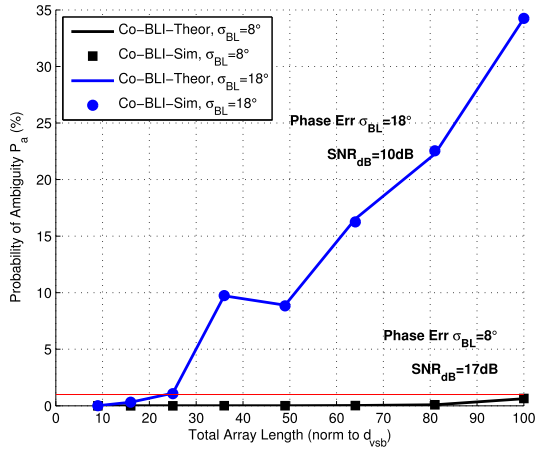

Fig. 8. Probability of ambiguity $P_a(\%)$ of a four-element Co-BLI versus total array length (norm to d_{vsb}).[legend: -Theor: theoretical; -Sim: simulation].

decrease SNR). Fig. 7 shows the corresponding plots, for the proposed Co-BLI as well as for the EPL, EPR, and MP (BLI) arrays. Similar to above, the Co-BLI together with the MP array again outperforms both EPL and EPR. Here also, the simulation results show fairly good match with the theoretical ones.

Lastly, we also simulate a four-element $n^2:mn:m(m+n)$ Co-BLI array, having antenna elements A_1, A_2, A_3, and A_4, with $d_{\text{vsb}} = 8.7$ mm to cover broadband of 2–18 GHz. For this, we consider two different SNR conditions, namely, 10 and 17 dB, and as before, for each of them, plot P_a vis-a-vis total array lengths through both simulation and theoretical calculations, as shown in Fig. 8. It is seen from Fig. 8 that as earlier, both simulation and theoretical results are having a good match. We also find that at SNR 10 dB, total normalized array length can be up to 25 to maintain P_a below 1%, while, for higher SNR, say, 17 dB, it can be extended to even 100. Now, from Fig. 3, the $n^2:mn:m(m+n)$ array considered above, has two $n:m:m+n$ Co-BLI arrays, namely, $A_1 - A_2 - A_3$ and $A_1 - A_3 - A_4$ acting in parallel in level-1. Thus, the probability of correct ambiguity resolution jointly at the first level will be $(1 - P_{a,CoBLI:3})^2$, where $P_{a,CoBLI:3}$ denotes the probability of ambiguity in each of the two Co-BLI triplets in level-1. It is easy to see that no ambiguity in the Co-BLI triplets in level-1 implies zero ambiguity in the subsequent normal BLI triplet $A_1 - A_3 - A_4$ in level-2, since, from (17), the former requires $\left|(m+n)\cdot e_{13} - n\cdot e_{14}\right| < n\pi$, while the latter requires $\left|(m+n)\cdot e_{13} - n\cdot e_{14}\right| < (m+n)\pi$ (here we use $e_{i,j}$ to denote the phase error between antennas A_i and A_j). Clearly, the latter is satisfied if the fomer holds true. Thus, the overall probability of ambiguity of the $n^2:mn:m(m+n)$ array is $1-(1-P_{a,\text{CoBLI:3}})^2 = 2P_{a,\text{CoBLI:3}} - P^2_{a,\text{CoBLI:3}}$ which is greater than $P_{a,\text{CoBLI:3}}$ and is approximately $2P_{a,\text{CoBLI:3}}$ for small $P_{a,\text{CoBLI:3}}$. This shows that under the same SNR conditions, as we move from a three-antenna Co-BLI array to a four-antenna Co-BLI array, the probability of ambiguity increases (maximally by a factor 2). However, the overall length of the array, and thus, the estimation accuracy increase by a much larger factor of $m+n$. This is validated in the above simulations (Figs. 6 and 8), where under the same SNR of 10 dB, P_a of 0.5% is attained by the three-element array with length $5d_{\text{vsb}}$ while <1% is attained by the four-element array of length as high as $25d_{\text{vsb}}$.

We also coded the proposed $2:3:5$ Co-BLI for three- and four-element Co-BLI arrays in VHDL language for Artix-7 series FPGA (Part No. XC7A200-11FFG -2). The circuit implementing (6) to find out R_{23} and R_{35} was made free of multipliers ($\times 2$, $\times 3$, and $\times 5$) using "single constant multiplication (SCM)" scheme [16]. The M-CAT table was mapped to block read-only-memory (BROM) in the FPGA and the design was made fully pipelined to reduce critical-path. Synthesis, implementation and placing and routing were carried out through Xilinx Vivado 2016.4 suite. The achievable max. clock frequency was found to be 444.4 MHz, meaning minimum clock period T_s of 2.25 ns. However, to maintain a safe margin, the design was run with a 250 MHz clock ($T_s = 4$ ns). The performance enhancement of the Co-BLI triplet is achieved at the cost of approximately 50% extra FPGA resources, as shown in Fig. 9, in comparison with normal BLI. The additional resources needed are, however, insignificant (<1%) compared to the overall available FPGA resources. Fig. 10 shows antenna array configurations having inter-element distances of 96 mm:64 mm in the 2–6 GHz three-antenna array and 86.7 mm:52 mm:78 mm in the 2–18 GHz four-antenna array. Here, d_{vsb} is taken as 32 mm for the three-element array and 8.7 mm for the four-element array to accommodate antennas having diameters 61.7 mm (2–6 GHz) and 50 mm (2–18 GHz), respectively, as well as to meet other design paramters.

We have evaluated the RMS DOA estimation error using the above setup in a radiation-mode environment inside a laboratory, created as per [17]. Here, the transmitter is kept fixed and the receiver is kept on a movable positioner

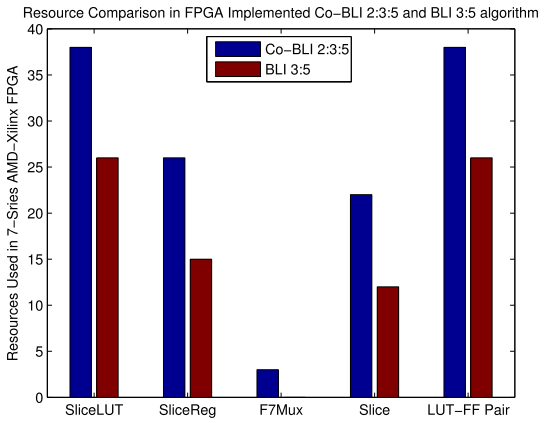

Fig. 9. Post P&R (place and route) implementation: FPGA resource comparison between Co-BLI and normal BLI.

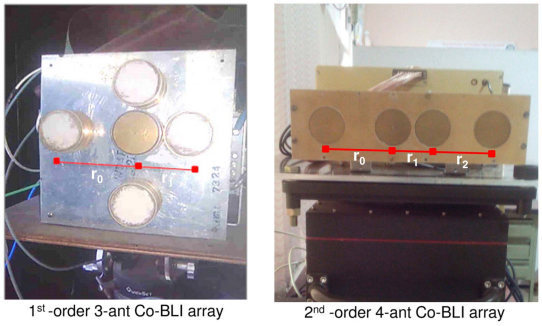

Fig. 10. Proto experimental setup showing Co-BLI array with (a) three-antenna (2:3) covering 2–6 GHz, (b) four-antenna (10:6:9) covering 2–18 GHz.

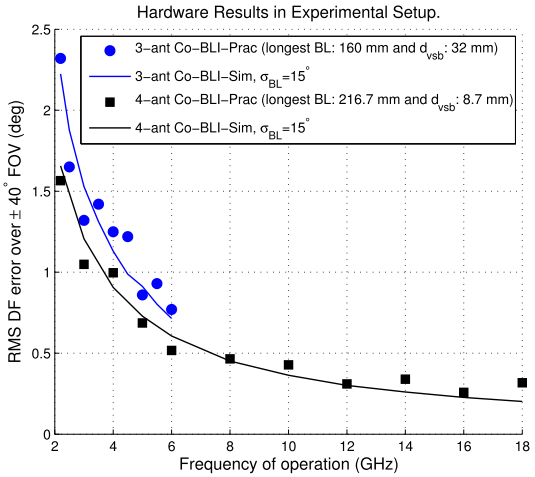

Fig. 11. RMS DOA estimation error obtained experimentally from three-antenna (2–6 GHz) and four-antenna (2–18 GHz) Co-BLI hardware. [legend: -Prac: practical; -Sim: simulation].

at a distance of 13 m approximately. The radio frequency of transmission having pulse width 800 ns with repetition period of 1 ms is varied at the steps of 500 MHz from 2–18 GHz. The RMS DOA estimation error observed experimentally over 2–6 GHz (three-element) and 2–18 GHz (four-element) are plotted against frequency using dotted sequence in Fig. 11, where we also plot MATLAB-based simulation results on the variation of the RMS DOA estimation error against frequency. Both are in good agreement as can be easily seen from Fig. 11. For the latter, we have taken $\sigma_{BL} \approx 15^{\circ}$ to account for phase errors of all hardware components (e.g., antenna, RF front end, etc).

VI. CONCLUSION

In this article, we have developed the *Co-BLI triplet* for a three-element BLI array which provides optimal performance for switched-element receiver or equivalent configurations. We have also generalized and extended the algorithm to work for four or more antenna BLI array with enhanced aperture length for higher DOA accuracy. A simple look-up-table based real-time implementation has been presented for the same through the M-CAT table. Finally, we have validated the proposed method through extensive MATLAB simulation results and also implemented in real-time FPGA based hardware.

ACKNOWLEDGMENT

The authors would like to thank Shri. N. Srinivas Rao, DS & Director-DLRL, Shri M. K. Das, Sc.G (retd.), Dr. M. Chakravarthy, OS & team, DLRL for their the unfailing support received throughout the course of this work.

REFERENCES

[1] A. De Martino, *Introduction to Modern EW Systems*. Boston, MA, USA: Artech House, 2012.
[2] S. Robertson, *Practical ESM Analysis*. Boston, MA, USA: Artech House 2019.
[3] S. E. Lipsky, *Microwave Passive Direction Finding*. Raleigh, NC, USA: SciTech Publishing, 2004.
[4] S. Chandran, *Advances in Direction of Arrival Estimation*. Boston, MA, USA: Artech House, 2006.
[5] R. L. Goodwin, "Ambiguity-resistant three and four-channel interferometers," Naval Res. Lab., Washington, DC, USA, NRL Report 8005, Sep. 1976.
[6] K.R. Sundaram, R.K. Mallik, and U. M. S. Murthy, "Modulo conversion method for estimating the direction of arrival," *IEEE Trans. Aerosp. Electron. Syst.*, vol. 36, no. 4, pp. 1391–1396, Oct. 2000.
[7] J. Lee, J. Lee, and J. Woo, "Method for obtaining three and four-element array spacing for interferometer direction-finding system," *IEEE Antennas Wireless Propag. Lett.*, vol. 15, pp. 897–900, 2016.
[8] J. Lee, J. Kim, H. Ryu, and Y. Park, "Mutliple array sapcings for an interferometer direction finder with high direction-finding accuracy in a wide range of frequencies," *IEEE Antennas Wireless Propag. Lett.*, vol. 17, no. 4, pp. 563–566, Apr. 2018.
[9] W. Horng, "An efficient DOA algorithm for phase interferometers," *IEEE Trans. Aerosp. Electron. Syst.*, vol. 56, no. 3, pp. 1819–1828, Jun. 2020.
[10] W. Wu, C. C. Cooper, and N. A. Goodman, "Switched-element direction finding," *IEEE Trans. Aerosp. Electron. Syst.*, vol. 45, no. 3, pp. 1209–1217, Jul. 2009.
[11] D. P. Palanivelu and M. Oispuu, "Calibration of antenna array with dual channel switched receiver system," in *Proc. 27th Eur. Signal Process. Conf.*, 2019, pp. 1–5.
[12] J. Lee and J. Woo, "Interferomter direction-finding system with improved DF accuracy using two different array configurations," *IEEE Antennas Wireless Propag. Lett.*, vol. 14, pp. 719–722, 2015.
[13] G. H. Hardy and E. M. Wright, *An Introduction to the Theory of Numbers*, 5th ed. Oxford, England: Clarendon Press, 1979.
[14] U. Dudley, *Elementary Number Theory*, 2nd ed. Mineola, NY, USA: Dover, 2008.

[15] H. Kim, "Antenna for active-passive seeker," South Korea Patent KR101619375B1, 2016.
[16] J. Thong and N. Nicolici, "An optimal and practical approach to single constant multiplication," *IEEE Trans. Comput.-Aided Des. Integr. Circuits Syst.*, vol. 30, no. 9, pp. 1373–1386, Sep. 2011.
[17] S. Samanta, M. K. Das, and M. Chakraborty, "A simple laboratory setup to create 2-D angle of arrival scenario keeping transmitter fixed and receiver moving on 3-axes servo," in *Proc. IEEE Int. Microw. RF Conf.*, 2014, pp. 373–376.

Sounak Samanta (Member, IEEE) received the B.E. degree in electronics engineering (gold medal) from the Sardar Vallabhbhai National Institute of Technology, Surat, Gujarat, India, in 2006, and the M.Tech. degree in electronics and electrical communication engineering, in 2013, from the Indian Institute of Technology Kharagpur, West Bengal, India, where he is currently working toward the Ph.D. degree in the area of designing algorithms and architectures for estimation of radar pulse parameters in modern electronic support receivers.

He joined the Defence Electronics Research Laboratory (DLRL-DRDO), Hyderabad, Telangana, India, in 2006, as a Scientist-B, where he is currently a Scientist-E. His research interests include frequency and direction of arrival estimations for modern electronic warfare receivers, digital beam forming and VLSI signal processing.

Mr. Samanta is a Life Member of the Indian Science Congress Association (ISCA), the Indian Society for Technical Education (ISTE), the Institution of Electronics and Telecommunication Engineers (IETE) and Member of the Association of Old Crows (AOC)-USA. He was the recipient of the Keshab K Parhi Endowment award by IIT Kharagpur in 2013 for best M.Tech thesis, the DLRL Technology Group award in 2008, DLRL Young Scientist award in 2015, and the DRDO Young Scientist award in 2018 for his significant contributions toward design of various frequency and direction of arrival estimation algorithms for defence applications.

Mrityunjoy Chakraborty (Senior Member, IEEE) received the B.E. degree in electronics and telecommunication engineering from Jadavpur University, Kolkata, India, in 1983, the M.Tech. degree in electrical engineering from the Indian Institute of Technology Kanpur, India, in 1985, and the Doctor of Philosophy degree in electrical engineering from the Indian Institute of Technology Delhi, New Delhi, India in 1994.

In 1994, he joined the Department of Electronics and Electrical Communication Engineering, Indian Institute of Technology Kharagpur, India, as a Lecturer, where he currently holds the position of Prithviraj Banerjee and Swati Banerjee Chair Professor, apart from being the Chair of the department. His research interests include digital and adaptive signal processing, linear algebra, optimization and compressive sensing, graph signal processing.

Dr. Chakraborty is a Fellow of the National Academy of Sciences, India, and Indian National Academy of Engineering (INAE). In 2019, he was the recipient of prestigious Chair Professorship of the INAE. Currently, he is an Associate Editor for IEEE TRANSACTIONS ON CIRCUITS AND SYSTEMS, PART II. Earlier, he was a Senior Editorial Board (SEB) Member of the *IEEE Signal Processing Magazine* during 2017–2020, an Associate Editor for IEEE TRANSACTIONS ON CIRCUITS AND SYSTEMS-I during 2004–2007 and 2010–2012, and of IEEE TRANSACTIONS ON CIRCUITS AND SYSTEMS II during 2008–2009, apart from being an SEB Member of IEEE JOURNAL ON EMERGING TECHNIQUES IN CIRCUITS AND SYSTEMS during 2016–2017. He has also been a Guest Editor of EURASIP Journal on Advances in Signal Processing and Special Issues of IEEE TRANSACTIONS ON CIRCUITS AND SYSTEMS II. During 2016–2018, he was the Chair of the DSP Technical Committee (TC) of the IEEE Circuits and Systems Society. He has also been a DSP Track Co-Chair of ISCAS 2015–2023, TPC Co-Chair of IEEE SIPS- 2018, Special Session Co-Chair of DSP-18, and Gabor Track Chair of DSP-15. He is a Co-Founder of the Asia Pacific Signal and Information Processing Association (APSIPA), and he was a Member of the APSIPA BOG during 2013–2016 and the Chair of the APSIPA TC on Signal and Information Processing Theory and Methods. In 2012 and 2020, he was the General Chair of the National Conference on Communications. During 2012–2013, he was selected as a Distinguished Lecturer of the APSIPA.